34

Prospective Techniques for Magnetic Resonance Imaging−Guided Robot-Assisted Stereotactic Neurosurgery

Ziyan Guo[1], Martin Chun-Wing Leong[1], Hao Su[2], Ka-Wai Kwok[1], Danny Tat-Ming Chan[3] and Wai-Sang Poon[3]

[1]The University of Hong Kong, Hong Kong
[2]City University of New York, New York City, NY, United States
[3]The Chinese University of Hong Kong, Hong Kong
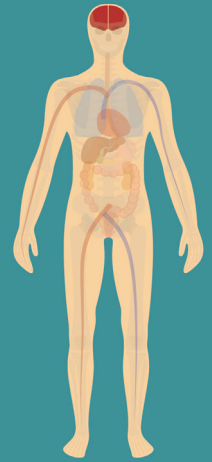
CHAPTER FOCUS
ENGINEERING & CLINICAL

TECHNOLOGY
ROBOTIC & IMAGE-GUIDED

LINK TO
VIDEO

ABSTRACT

Stereotactic neurosurgery involves a technique that can locate the brain targets using an external coordinate system. With the advancements of magnetic resonance imaging (MRI), numerous studies on frameless stereotaxy and MRI-guided/verified technique have been reported to improve the workflow and surgical outcomes. Intraoperative (intraop) MRI guidance in frameless techniques is an appealing method which could simplify workflow by reducing the coregistration errors in different imaging modalities and monitoring the surgical progress. Manually operated platforms thus emerge for MRI-guided frameless procedures. However, these procedures could still be complicated and time-consuming due to their intensive manual operation. To further simplify the procedure and enhance accuracy, robotics has been introduced. In this chapter, we review the state-of-the-art intraop MRI-guided robotic platforms for stereotactic neurosurgery. To improve surgical workflow and achieve greater clinical penetration, three key enabling techniques are discussed with emphasis on their current status, limitations, and future trends.

BRAIN

34.1 Background

Stereotactic neurosurgery requires locating the targets of interest within the brain using an external coordinate system [1]. Stereotactic approaches have been adopted in a wide variety of procedures, such as biopsy, ablation, catheter placement, stereo electroencephalography, and deep brain stimulation (DBS) [2−4]. Three key stages are incorporated in current stereotaxy workflow: (1) *preoperative* (*preop*) *planning* which provides a roadmap to the interventionists prior to the operation; (2) *immediate planning* which involves registering the three-dimensional (3D) coordinates of a stereotactic frame onto the preop image; and (3) *intraoperative* (*intraop*) *refinement* which involves setting up the system for intervention.

Preop planning involves high-resolution tomography, such as computed tomography (CT) and magnetic resonance (MR) imaging (MRI). These imaging modalities offer crucial image accuracy for precise target/lesion localization. In particular, MRI (e.g., gadolinium-enhanced MR images) is advantageous to visualize deep brain structures for the treatment of functional disorders. Special MRI sequences can also be used to pinpoint the target/lesion location on the 3D roadmap. After locating the required region-of-interests, *immediate planning* involves the realignment of the frame through image fusion and registration. Such realignment is crucial to obtain a consistent coordinate system among the frame and the preop roadmap. Finally, *intraop refinement* involves essential procedures such as the creation of a burr hole for dural puncture. For DBS, microelectrode recording (MER) and macrostimulation are also involved in this stage for physiological validation.

Instrument manipulation for stereotactic neurosurgery remained a major challenge, despite the standard workflow that has been established for multiple decades. Satisfying the supreme demand of precision while minimizing invasiveness is the key to successful operation. Imprecise positioning of instruments would result in deviated trajectory and targeting error, which would significantly increase the risk of hemorrhage. Although image fusion (registration) has been performed at the immediate planning stage, it cannot compensate for the dynamically changing condition during surgery. Particularly, the unavoidable brain shift/deformation after craniotomy can affect the position of the critical/target regions on the brain. Many procedures can also cause brain shift, such as instrument manipulation, anesthesia operation, change in intracranial pressure, postural/gravitational forces, tissue removal and effect of pharmaceuticals. Given the multiplexed causes of brain shift, solely using the preop images as a roadmap is undesirable. Continuous updates are therefore required. The incorporation of advanced real-time visualization is crucial for precise instrument manipulation and brain shift compensation.

The advances in intraop imaging techniques, particularly intraop MRI, simplify the perplexing workflow for stereotactic neurosurgeries. MRI possesses several advantages over other modalities (e.g., CT or ultrasound) thanks to its high sensitivity for intracranial physiological/pathological changes and its capability of visualizing soft tissues in high contrast without radiation. To date, MR images can be acquired swiftly through advanced radiofrequency excitation sequences (e.g., fast imaging with low angle shot sequence can achieve a temporal resolution of 20−30 ms [5]). These imaging techniques, which permit real-time guidance on soft-tissue deformation, can be supported in many current MRI facilities. With increasing real-time MRI availability, there is sufficient support for MRI-guided robots to find their way into more complex surgical procedures. These MRI robots are capable of delivering more precise treatment through accurate image guidance. Device implantation and tissue ablation are timely examples. In this review, we provide a discussion regarding the state-of-the-art apparatus and MR safe/conditional robots for stereotactic neurosurgery, as well as the key enabling techniques, with emphasis on their current status, limitations, and future trends.

34.2 Clinical motivations for magnetic resonance imaging−guided robotic stereotaxy

Computer-aided navigation systems have enabled intraop guidance based on preop images since the 1990s (Fig. 34.1) [6]. The advancement of intraop navigation techniques enables frameless stereotaxy, which utilizes fiducial landmarks to replace the rigid frame for registration and transformation of the frame-of-reference. With the fiducial markers/contours providing real-time positional information of the imaged brain and the surgical instrument, the accuracy [7−10], diagnostic yield, morbidity, and mortality rate [11] of frameless stereotaxy are currently comparable to its frame-based counterpart. In addition, frameless stereotactic neurosurgery is also associated with reduced anesthetic time and fewer complications [12].

Despite frameless instrument guidance being achieved, intraop continual visualization of the surgical process remains a challenge [13−15]. Taking the conventional DBS as an example, it utilizes MER and fluoroscopy/CT images concurrently to confirm the placement location of the electrodes. The patient, however, is required to stay awake
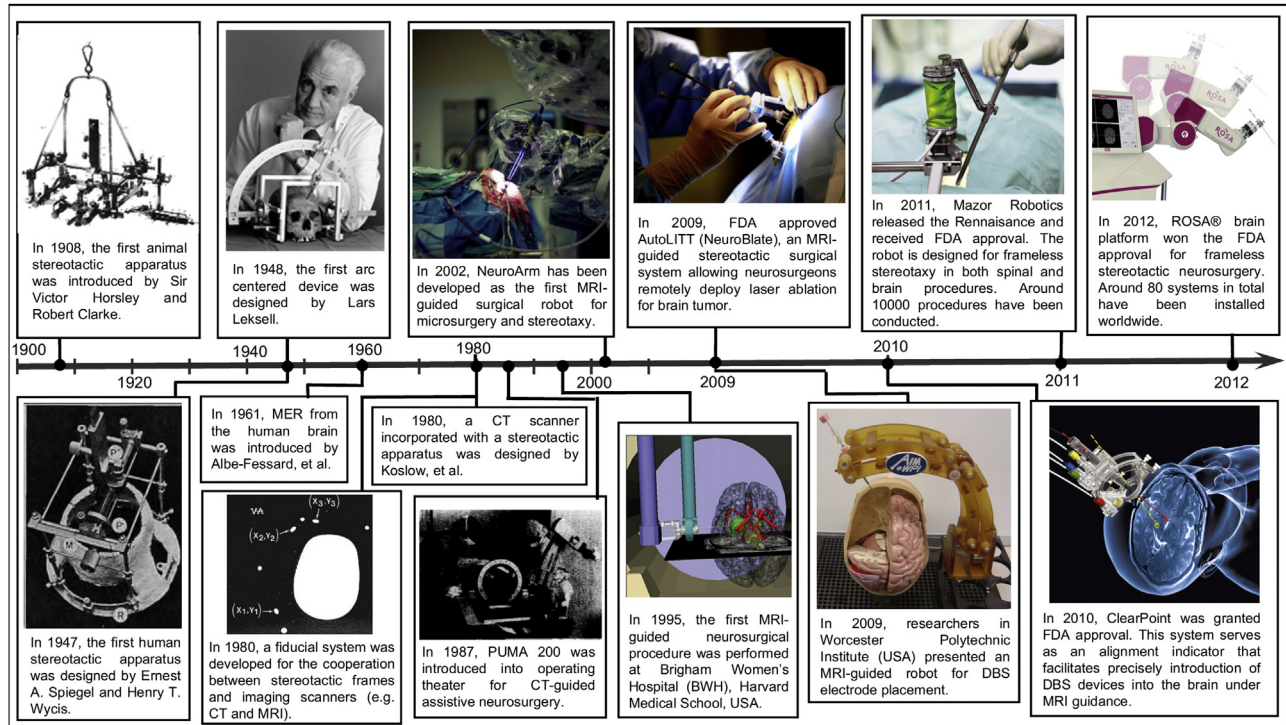
FIGURE 34.1 Key milestones of stereotactic devices for image-guided neurosurgery.

throughout the surgery under local anesthesia for the interventionists to assess the corresponding symptoms [16]. Coregistering fluoroscopy images with the preop roadmap is susceptible to registration errors. In this light, intraop MRI is the preferred imaging modality thanks to its sensitivity to intracranial pathology with high-contrast soft-tissue images. The resultant images in 3D can provide the surgical navigation system with clear visualization, allowing precise guidance of the instrument to the target tissue in real-time. By incorporating MRI guidance in the frameless stereotaxy technique, the multiplexed workflow of DBS can be further streamlined by conducting general anesthesia and verification in situ with MR images [17]. The patient need not stay awake in response to the interventionists. The instrumental position can also be pinpointed throughout the surgical process [18].

34.3 Significant platforms for magnetic resonance imaging−guided stereotactic neurosurgery

Manually operated stereotactic platforms have been developed for MRI-guided neurosurgeries, such as the NexFrame (Medtronic, Inc., United States) and the SmartFrame (ClearPoint, MRI Interventions, Inc., United States) [24] systems. Notably, the ClearPoint system (Fig. 34.2A) has been deployed for several therapeutic approaches including electrode placement [25], focal ablation [26] and direct drug delivery [27]. These MR-safe/conditional platforms have been validated through a number of clinical trials [16,28,29]. Particularly, there was a clinical study on frameless DBS approaches involving 27 patients with movement disorders [17]. This study clearly indicated that frameless DBS under MRI guidance can reduce procedural time without sacrificing surgical accuracy. However, patients have to be moved in and out of the scanner's isocenter for imaging updates and manual instrument adjustment. Such a requirement not only increases the operation time, but also demands advanced peripherals such as a compatible anesthesia system. These challenges have directed increasing attention at developing intraop manipulators and further translating robotics technology into neurosurgery. Robots can be superior over humans in certain areas, especially for intensive, tedious tasks that demand high precision. Having a compact robot capable of operating inside the confined MRI bore also mitigates the disturbing requirement of frequent patient transfer to/from the isocenter. The increasing demands of MRI-guided robotic platforms for stereotactic neurosurgeries can also be inferred by the rising number of recent reports [30−32]. The clinical benefits of such platforms are extensively discussed.

FIGURE 34.2 Significant MRI-guided stereotactic neurosurgical systems. (A) ClearPoint system by MRI Interventions, Inc., United States. Two frames (SmartFrame) are mounted to the skull bilaterally and manually aligned to the predefined trajectories [18,19]; (B) MRI-compatible surgical assist robot by AIST-MITI, Japan and BWH, Harvard Medical School, United States [20]; (C) NeuroArm/SYMBIS by Deerfield Imaging, United States [21]; (D) NeuroBlate system by Monteris Medical, Inc., United States [22]; (E) a MRI-guided stereotactic robot for deep brain stimulation, developed by Worcester Polytechnic Institute, United States [23]. *MRI*, Magnetic resonance imaging.

Fig. 34.2B illustrates the early models of MR conditional robots such as those presented in Masamune et al. [33] and Chinzei et al. [34]. These early robot prototypes have a large footprint in the operating room, and are mostly based on low-field, open-bored interventional MRI (iMRI) scanners (e.g., Signa SP 0.5T, GE Medical Systems, United States). The robot reported in Chinzei et al. [34,35] is the first robotic platform integrated with an optically linked frameless stereotactic system. These early robot models have a few key disadvantages. Images obtained from specialized iMRI scanners often have impaired image quality due to the scanners having a low base magnetic field. Any metal-containing robot components can further degrade the already suboptimal image quality. Furthermore, most of these early robotic systems lack tele-operating capabilities, of which any manual influence on the system may be hindered by the confined iMRI workspace.

Fig. 34.2C illustrates NeuroArm/SYMBIS (Deerfield Imaging, United States), which is an MR-compatible robotic system for tele-operative microsurgery and stereotactic brain biopsy [36,37]. It consists of two 7 + 1 degrees of freedom (DoFs) manipulators and is able to operate with a maximum load of 0.5 kg. It also features a moderate force output and movement speed of 10 N and 0.5−5 mm/s, respectively [38]. These manipulators are semiactively controlled by a remote workstation integrated with hand tremor filter and movement scaling. Stereotaxy can be conducted within the magnetic bore using a single MRI-compatible robotic arm. This robot arm is fabricated with MR-compatible materials such as titanium, polyetheretherketone, and polyoxymethylene [21]. To provide a constant frame-of-reference for effective robot control, this MR-compatible robot arm is directly attached to the magnet bore.

Fig. 34.2D shows the Monteris stereotactic platform which is capable of tele-operating a two-DoF robotic device for laser ablation. The NeuroBlade laser probe is oriented by a separate, disposable MRI-compatible stereotactic frame (AXiiiS stereotactic miniframe) that is also visible on the MR images. This stereotactic frame consists of three translatable legs and a ball socket for the instrument to engage the treatment target from any angle. The laser fiber for ablation is oriented and driven by piezoelectric motors. Utilizing real-time MRI and thermometry data, the surgeon can monitor and update the probe position and ablation profile accordingly [39]. However, if multiple ablations are required, the patient may be required to be transferred back to the operation theater for probe removal, frame realignment, and possibly new craniotomy.

Finally, Fig. 34.2E illustrates a recent research prototype developed by Fischer et al. [23,40], which is designed specifically to place DBS leads under the guidance of MRI. The system features six DoFs driven by piezoelectric motors, which mimics the functionality and kinematic structure of a conventional stereotactic frame (e.g., Leksell frame). It has been demonstrated that the simultaneous robotic manipulation and imaging would not affect the imaging usability for visualization and navigation. The robot could reach targets in a static phantom model with accuracy 1.37 ± 0.06 mm in tip position and 0.79 ± 0.41 degree in insertion angle [40].

34.4   Key enabling technologies for magnetic resonance imaging−guided robotic systems

The goal of MRI-guided stereotactic neurosurgical platforms is to achieve higher accuracy, effectiveness, and optimized surgical workflow. Despite there being many developed MRI-guided robotic systems (as listed in Table 34.1), only a few of them are available on the market; achieving widespread clinical use is still an ambitious objective. Furthermore, adopting MRI-guided robotic systems also introduces additional costs. Particularly, the expenses of occupying the MRI suite for a prolonged time can be substantial, let aside the expensive MRI-compatible instruments [12]. These associated costs can be detrimental to the application of MRI-compatible robotics in health care [58]. Streamlining the surgical workflow may be a way out to enable widespread application. Here we propose three key enabling technologies for high-performance intraop MRI-guided robotic platforms, which would simplify the workflow (as illustrated in Fig. 34.3) and potentially reduce the surgical costs.

TABLE 34.1 Existing robotic systems for magnetic resonance (MR) imaging (MRI)-guided neurosurgery.

Emerging platforms	Degrees of freedom	Number of end effectors	Actuator[a]	Accuracy	HMI	Features	Key references
NeuroArm/ SYMBIS (Deerfield Imaging, United States)	7 + 1	2	E	Submillimeter	√	Tele-operated microsurgery and stereotaxy Only one manipulator can fit into the magnet bore Haptic feedback 3D image reconstruction for navigation Phase: FDA approved, commercial	Sutherland et al. [41]; Louw et al. [42]; Motkoski et al. [21]
NeuroBlate (Monteris Medical, Inc., United States)	2	1	E	1.57 ± 0.21 mm	√	Laser ablation Patient under general anesthesia Continuous MR thermography acquisition Phase: FDA approved, commercial	Mohammadi et al., 2014 [44]; Manijila et al., 2016 [43]
Pneumatic MRI-compatible needle driver (Vanderbilt University, United States)	2	1	P	1.11 mm	−	Transforamenal ablation; Precurved concentric tube 3T closed-bore MRI scanner Phase: clinical trial	Comber et al. [45,46]
MRI-guided surgical manipulator (AIST-MITI, Japan and BWH, Harvard University, United States)	5	1	E	0.17 mm/ 0.17 degree	−	Navigation and axisymmetric tool placement 0.5T open MRI scanner Pointing device only; Phase: in vivo test with a swine brain	Chinzei et al. [47]; Koseki et al. [48]

(Continued)

34. Stereotactic NeuroSurgery

TABLE 34.1 (Continued)

Emerging platforms	Degrees of freedom	Number of end effectors	Actuator[a]	Accuracy	HMI	Features	Key references
MRI-compatible stereotactic neurosurgery robot (Worcester Polytechnic Institute, United States)	7	1	E	1.37 ± 0.06 mm	–	Needle-based neural interventions Mounted at the MRI table SNR reduction in imaging less than 10.3% Phase: research prototype	Li et al. [23]; Nycz et al. [40]
Mesoscale neurosurgery robot (Georgia Institute of Technology, United States)	[b]	1	[c]	About 1 mm	–	Tumor resection, hemorrhage evacuation Skull-mounted Phase: research prototype	Ho et al. [49]; Kim et al. [50]; Cheng et al. [51]
MR safe bilateral stereotactic robot (The University of Hong Kong, Hong Kong)	8	2	H	1.73 ± 0.75 mm	–	Bilateral stereotactic neurosurgery Skull-mounted MR safe/induce minimal imaging interference Phase: research prototype	Guo et al. [52]
Multi-imager-compatible needle-guide robot (Johns Hopkins University, United States)	3	1	P	1.55 ± 0.81 mm	–	General needle-based interventions Table-mounted iMRIS Phase: research prototype	Jun et al. [53]
MRI-compatible needle insertion manipulator (University of Tokyo, Japan)	6	1	E	3.0 mm	–	Needle placement 0.5T MRI scanner Phase: research prototype	Masamune et al. [33]; Miyata et al. [54]
Endoscope manipulator (AIST, Japan)	4	1	E	About 0.12 mm/ 0.04 degree	–	Endoscope manipulation for transnasal neurosurgery Vertical field open MRI Large imaging noise caused by ultrasonic motors Phase: research prototype	Koseki et al. [55]
Tele-robotic system for MRI-guided neurosurgery (California State University, United States and University of Toronto, Canada)	7	1	P/H	–	√	Brain biopsy 1.5T MRI scanner Mounted at the surgical table Phase: research prototype	Raoufi et al. [56]

(*Continued*)

TABLE 34.1 (Continued)

Emerging platforms	Degrees of freedom	Number of end effectors	Actuator[a]	Accuracy	HMI	Features	Key references
Open-MRI compatible robot (Beihang University, China)	5	1	E	–	–	Biopsy and brachytherapy 0.3T iMRIS Phase: research prototype	Hong et al. [57]

3D, Three-dimensional; *FDA*, Food and Drug Administration; *HMI*, human−machine interface; *iMRIS*, Intraoperative MRI scanner.
[a]*Actuator: E, nonmagnetic electric actuator, such as piezoelectric motor or ultrasonic motor; P, pneumatic actuator; H, hydraulic actuator.*
[b]*A flexible continuum robot, of which the degrees of freedom depend on the number of segments.*
[c]*Shape memory alloy spring-based actuators remotely driving the manipulator via pulling tendons.*
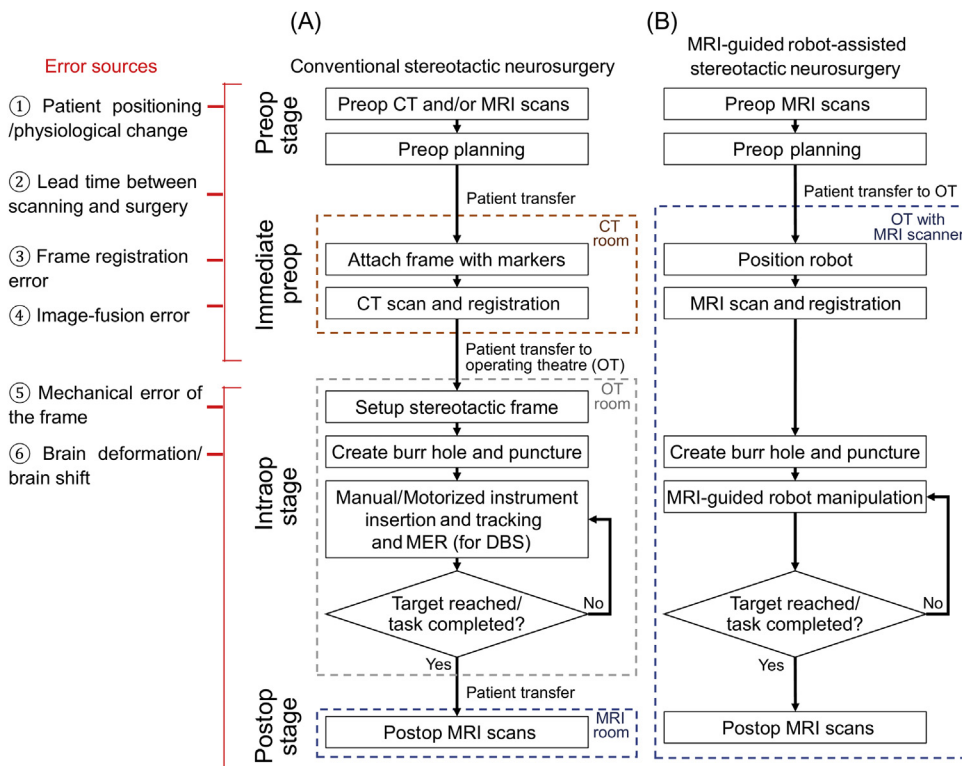

FIGURE 34.3 Workflow of (A) conventional stereotactic neurosurgery; (B) MRI-guided robotic neurosurgery. In the robot-assisted procedure, errors can be mitigated by the guidance of real-time MRI and closed-loop control of robotic manipulation. *MRI*, Magnetic resonance imaging.

34.4.1   Nonrigid image registration

Mismatch between the preop and intraop images can lead to much confusion in the process of target localization. Such a mismatch can arise from various sources: (1) differences in patient positioning during scanning and surgery (e.g., in supine/prone); (2) lead time between scanning and surgery; (3) number of sampling fiducial points for registration; and (4) intrinsic error in image fusion. Image registration mitigates such misalignments, thus enabling precise localization of the preoperatively segmented critical/target regions on the intraop images. With the target location pinpointed on the rapidly acquired intraop image, the surgical plan can be established/updated accordingly. To date, many commercial navigation systems only employ *rigid* registration to realign the both sets of images. However, it cannot compensate for any image discrepancy resulting from the actual brain deformation and the MR image distortion. For example, it cannot tackle the severe misalignment ($\sim 10-30$ mm [59]) caused by brain shift after craniotomy (Fig. 34.4). This large-scale
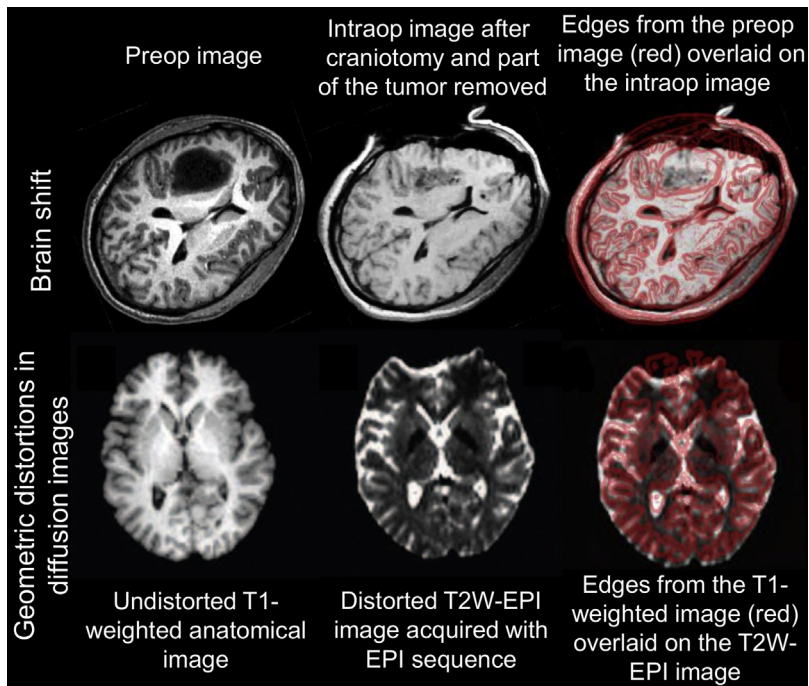
FIGURE 34.4 (Upper row) Brain deformation before and after the craniotomy [60]; (lower row) geometric distortion in diffusion images [71].

brain deformation inevitably makes the surgical plan inconsistent with the actual anatomy during the procedure. *Nonrigid* image registration has been proposed to mitigate such misalignment. In particular, the biomechanical finite-element-based registration schemes are specifically developed to estimate and predict the extension of any brain shift of different regions. The relative stiffness model of intracranial structures has to be constructed so as to deduce deformation caused by gravity [60−62].

Apart from nonlinear image discrepancy due to the tissue deformation, spatial distortion of MR images would also hamper the accuracy in MRI-guided stereotactic surgery [63]. The cause of MR distortion is multiform and incalculable. Let alone base (static) field inhomogeneity, chemical shift, and susceptibility artifacts, the nonlinearity of the B1 gradient field contributes most to such distortion. It has been reported that the spatial distortions can be as much as 25 mm at the perimeter of an uncorrected 1.5T MR image; the error would still remain within the 1% range (typically ~ 4 mm) even after standard gradient calibration using a grid phantom [64,65]. This error is significant concerning the supreme accuracy requirement in stereotaxy. Worse still, the distortion may even be aggravated due to the higher magnetic field inhomogeneity that presents in 3T MRI scanners [63]. The combined effect of these variables often results in very complex and nondeterministic image distortion, particularly affecting the images obtained by advanced excitation sequences. For example, the echo-planar imaging sequence used in the acquisition of diffusion-weighted images is vulnerable to susceptibility-induced distortions, resulting in heavy distortion at the tissue margins where the magnetic susceptibility is rapidly changing in 3D space (Fig. 34.4) [66].

Considering such gradient field nonlinearity, gradient-based excitation sequences are set back despite its widespread usefulness. *Nonrigid* registration schemes can correct the distortion in gradient-based image while retaining any useful anatomical information. This can be achieved by registering the distorted image to a standard MR image (e.g., T2 turbo spin echo images that exhibit little image distortion) obtained at the same imaging instance. As a result, the image correspondence in 3D obtained by nonrigid registration can reliably restore any misalignment caused by image distortion. Recent research demonstrated that significant ($> 10\%$) accuracy improvement has been archived by resolving such a misalignment [67]. However, complex computation involved in nonrigid registration schemes impedes its efficacy to be used in the intraop scenario. This motivates the development of high-performance image registration schemes using scalable computation architectures such as graphical processing units, field-programmable gate arrays, or computation clusters. Recent works [68−70] have demonstrated substantial computation speed up, in which the registration process can be accomplished within seconds, even with a large image dataset in 3D (~ 27 M voxels) being used.

34.4.2 Magnetic resonance−based tracking

Real-time tracking enables in situ positional feedback of stereotactic instruments inside the MRI scanner bore. Not only does it act as the feedback data to close the control loop of a robot, it also allows the operator to visualize the instrument position/configuration with respect to the brain roadmap. A sufficient number of tracked markers are required to pinpoint the instrument in the image coordinates [72]. However, real-time positional tracking of the instrument inside the MRI scanner is challenging for several reasons: (1) conventional instruments can either be invisible or create serious susceptibility artifacts on MR images; (2) restricted space of the scanner bore and complicated electromagnetic (EM)-shielding limit the use of external tracking devices, for example, stereo-optical cameras; and (3) image reconstruction is time-consuming (e.g., 9.440 seconds required for acquisition of a slice of T2-weighted MR image with field of volume of 220×220 mm [73]). Only a few 2D images can be obtained, therefore it is hard to localize multiple marker points on an image domain in relatively large 3D space.

Passive tracking (Fig. 34.5, upper row) is the most commonly used method, in which passive markers are incorporated with the stereotactic instruments and directly visible in MR images by changing the contrast. No additional hardware is necessary. The markers are either filled with paramagnetic agents (e.g., gadolinium compounds) that can produce positive MR image contrast, or diamagnetic materials (e.g., ceramic) that generates negative contrast. The shape of these markers can be customized into spheres, tubes, or other desired structures for the ease of recognition on the images. Passive tracking is simple and safe, and can be performed under various MR field strengths without inducing any heat. However, passive markers may be invalid when the markers are in close proximity, or out of the imaging slice [74]. Thus, the configuration of the marker system needs to be specially designed for ready identification [75]. In addition, the localization of passive markers is challenging to perform automatically and also in real time. The visualization of passive markers relies on 2D image reconstruction, which is time-consuming and may not be reliable as the MR images are intrinsically distorted [76].

To tackle these challenges, much research attention has been recently given to the MR-based active tracking techniques (Fig. 34.5, lower row). Active markers are small coils serving as antennas individually connected with the MRI scanner receivers, and actively respond to the MR gradient field along three principal directions. Without the need for
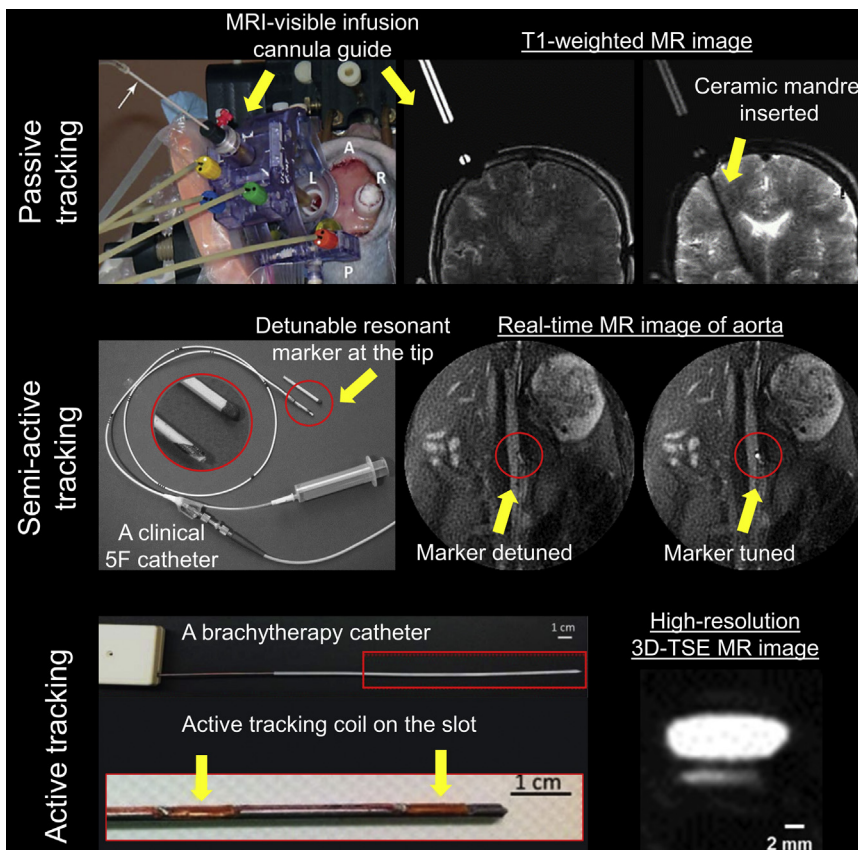

FIGURE 34.5 (Upper row) An MRI-visible guide oriented by a stereotactic device to align with the planned trajectory. A ceramic mandrel is inserted subsequently after the alignment and its tip position is validated in MR image [84,85]; (middle row) a 5 F catheter embedded with a semiactive marker at the tip. This marker is a resonant circuit and can be controlled by optical fiber. The two MR images show that the marker produces no signal enhancement in the detuned state and an intense signal spot in the tuned state [86]; (lower row) active markers mounted at a brachytherapy catheter. 3D TSE sequence is adopted to generate a high-resolution MR image (resolution: $0.6 \times 0.6 \times 0.6$ mm³) [83]. *3D*, Three-dimensional; *MRI*, magnetic resonance imaging; *TSE*, turbo spin echo.

34. Stereotactic NeuroSurgery

image reconstruction, the markers can be rapidly localized using a 1D projection technique [77]. This localization is automatic, since the marker can be independently identified through its own receiving channel [78,79]. The obtained coordinates may then be immediately used for adjustment of the further scanning plane [80]. Specific MR sequences are designed to incorporate and interleave both tracking and imaging. Delicate heat control is also needed because of the resonating RF waves and the storage of electrical energy caused by the conductive structure [81]. Therefore, a semi-active tracking system is also preferable, in which there is no electrical wire connected between the coil marker and the MRI scanner. It resolves the potential problem of heat generated by the wires. This marker unit acts as an RF receiver to pick up the MR gradient signal, as well as an inductor to resonate with the signal transmitted to the MRI scanner receiver [82]. The resonance frequency of this coil marker needs fine tuning to adapt with the scanners of different field strengths (i.e., 63.8 and 123.5 MHz, respectively, for 1.5 and 3T MRI scanners), while the 1.5T scanner is more popular in clinical practice and 3T can provide images with lower noise and a faster acquisition time.

We can foresee that such MR-based tracking coils could be implemented in stereotactic neurosurgery to realize real-time instrument tracking. Promising results have been reported in an MR-active tracking system for intraop MRI-guided brachytherapy. Three active microcoil markers (1.5×8 mm^2, Fig. 34.5) are mounted on a Ø1.6 mm brachytherapy stylet [83]. Both the tracking and imaging are in the same coordinate system, the stylet configuration can be virtually augmented on the MR images in situ. High-resolution ($0.6 \times 0.6 \times 0.6$ mm^3) stylet localization at high sampling rate (40 Hz) and low-latency (<1.5 ms) could be achieved.

34.4.3 Magnetic resonance imaging−compatible actuation

The actuator is another key component of a robot. Its performance also determines the surgical safety and accuracy, in particular for instrument manipulation in stereotactic surgery that involves precise coordination of three DoFs at least and demands an average accuracy of 2−3 mm. Conventional high-performance actuators mostly consist of magnets and are driven by EM power. However, the use of ferromagnetic materials is forbidden under a strong magnetic field. This poses a strong incentive to develop motors that are safe and compatible with the MRI environment. Piezoelectric motors actuated by high-frequency electric current have been extensively applied for iMRI applications [87−89]. Such motors are usually small in size (e.g., $40.5 \times 25.7 \times 12.7$ mm^3, Nanomotion motor as shown in Fig. 34.6, upper row), and can provide fine movement at the nanoscale. However, the motion range and speed of these motors are limited and insufficient for some long-stroke DoFs (e.g., inserting an ablation catheter for tumors located in the deep brain area) without
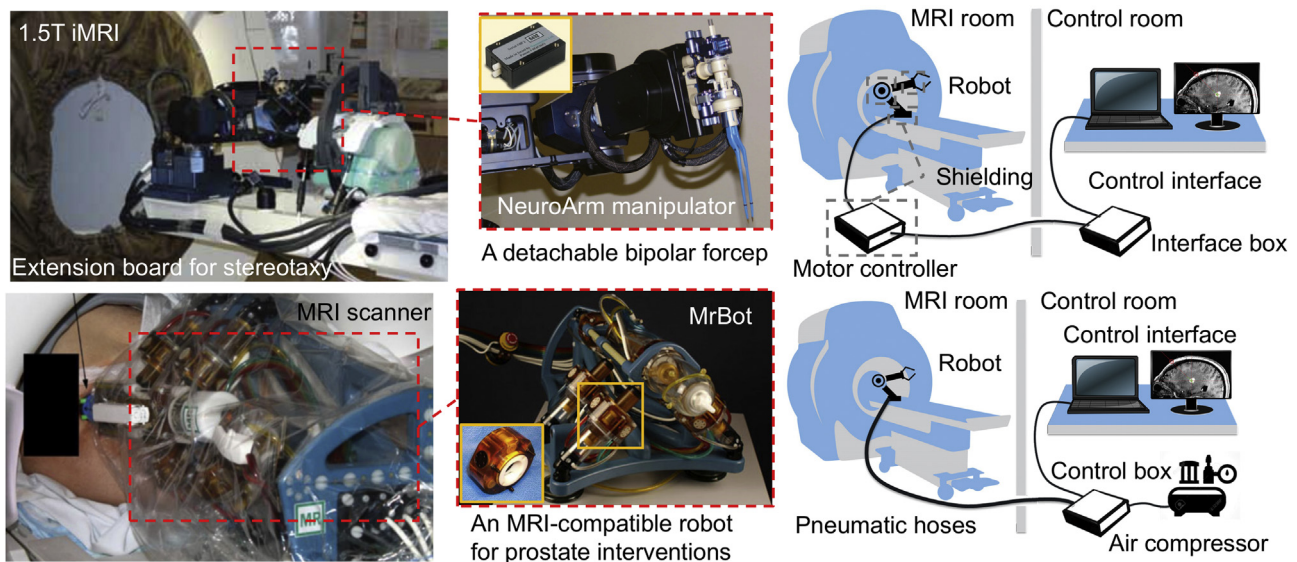

FIGURE 34.6 Exemplary MRI-compatible robotic systems driven by different motors. (Upper row) NeuroArm manipulator (in *red frame*) driven by ultrasonic piezoelectric motors (in *yellow frame*). The manipulator is mounted onto an extension board for stereotaxy [96,97]. Careful EM-shielding is required for the motors and controller box placed inside the MRI room to ensure safety and minimal interference to the imaging. System setup diagram of the robot integrated with ultrasonic motors is shown on the right. (Lower row) Prostate robot (in *red frame*) driven by pneumatic stepper motors (in *yellow frame*) [91,98]. The controller box can be placed in the control room and connected with the motors via air hoses. System setup diagram of the robot integrated with pneumatic motors is shown on the right. *EM*, Electromagnetic *MRI*, magnetic resonance imaging.

additional mechanisms. EM interference is inevitably induced by the high-frequency electrical signal. Tailormade EM shielding of the motor and its electronic drivers may degrade the motor compactness [88,90]. Nevertheless, the imaging quality can be more or less deteriorated by the presence of electric current while the motors operate inside the scanner bore during the image acquisition, thus affecting the visualization of small targets (e.g., DBS targets with diameters of approximately 4−12 mm).

In this light, intrinsically MR-safe motors driven by other energy sources, for example, pressurized air/water flow, are preferable. Minimal EM interference is generated by this fluid-driven actuation [91−94]. Fig. 34.6 (lower row) shows a general setup of a pneumatically actuated MRI robot. Long transmission air pipes (e.g., 10 m) connect the robot and its control box, which are placed in MRI and control rooms separately. Pressurized air at 0.2−0.4 MPa can be supplied from the medical air system commonly available in hospital rooms. However, the high-frequency air pulses may generate unfavorable noises and vibration in the operating room. The compressibility of air results in limited torque/force output and low-stiffness transmission, making the positional accuracy hard to reach the millimeter level and satisfy the requirement in stereotaxy [95]. In contrast, incompressible liquid (e.g., water, oil) in hydraulic motors offers relatively accurate, responsive, and steady mechanical transmission. They can typically render large output power. A master−slave design is usually adopted in hydraulic systems. The master unit is placed in the control room, which is driven by electric motors; the slave unit works near or inside the MRI scanner bore, which is made of MR-safe materials and its power is transmitted from the master unit via long hydraulic tubes. In this hydraulic system, discreet sealing for all the connectors is required to prevent liquid leakage. This may pose difficulties in setting up the robot, for example, when disconnecting and reconnecting the hydraulic tubes through the waveguide (with diameter of ∼∅100 mm) between the MRI room and the control room.

34.5 Conclusion

In this review, we have given an overview of the emerging robotic platforms for MRI-guided stereotactic neurosurgery. These neurosurgical systems allow for enhanced dexterity, stability, and accuracy beyond manual operation. However, few of them are in wide application. This may be due to the lack of optimized surgical workflow and outcomes to compensate for the high cost of using MRI and MRI-compatible instruments/robot. To tackle this challenge, three key enabling technologies have been proposed in this chapter, namely *nonrigid* image registration, MR-based positional tracking, and MR-safe actuation. All these technological developments will eventually serve to exploit the information and augment the surgeon's capabilities, by providing enhanced visualization and manipulation. Continued efforts to incorporate these techniques and evaluate the clinical benefits would be of great value.

References

[1] Galloway R, Maciunas RJ. Stereotactic neurosurgery. Crit Rev Biomed Eng 1989;18(3):181−205.

[2] Spiegel EA, Wycis HT, Marks M, Lee AJ. Stereotaxic apparatus for operations on the human brain. Science 1947;106(2754):349−50.

[3] Henderson JM, Holloway KL, Gaede SE, Rosenow JM. The application accuracy of a skull-mounted trajectory guide system for image-guided functional neurosurgery. Comput Aided Surg 2004;9(4):155−60.

[4] Gonzalez-Martinez J, Vadera S, Mullin J, Enatsu R, Alexopoulos AV, Patwardhan R, et al. Robot-assisted stereotactic laser ablation in medically intractable epilepsy: operative technique. Oper Neurosurg 2014;10(2):167−73.

[5] Uecker M, Zhang S, Voit D, Karaus A, Merboldt KD, Frahm J, et al. Real-time MRI at a resolution of 20 ms. NMR Biomed 2010;23(8):986−94.

[6] Mert A, Gan LS, Knosp E, Sutherland GR, Wolfsberger S. Advanced cranial navigation. Neurosurgery 2013;72(Suppl. 1):A43−53.

[7] Holloway KL, Gaede SE, Starr PA, Rosenow JM, Ramakrishnan V, Henderson JM. Frameless stereotaxy using bone fiducial markers for deep brain stimulation. J Neurosurg 2005;103(3):404−13.

[8] Henderson JM. Frameless localization for functional neurosurgical procedures: a preliminary accuracy study. Stereotact Funct Neurosurg 2004;82(4):135−41.

[9] Maciunas RJ, Fitzpatrick JM, Galloway RL, Allen GS. Beyond stereotaxy: extreme levels of application accuracy are provided by implantable fiducial markers for interactive image-guided neurosurgery. Interactive image-guided neurosurgery. Am Assoc Neurol Surg 1993; ISBN: 1879284154.

[10] Maciunas RJ, Galloway Jr RL, Latimer JW. The application accuracy of stereotactic frames. Neurosurgery 1994;35(4):682−95.

[11] Dammers R, Haitsma IK, Schouten JW, Kros JM, Avezaat CJ, Vincent AJ. Safety and efficacy of frameless and frame-based intracranial biopsy techniques. Acta Neurochir (Wien) 2008;150(1):23.

[12] Dorward NL, Paleologos TS, Alberti O, Thomas DG. The advantages of frameless stereotactic biopsy over frame-based biopsy. Br J Neurosurg 2002;16(2):110−18.

[13] Lunsford DL, Parrish R, Albright L. Intraoperative imaging with a therapeutic computed tomographic scanner. Neurosurgery 1984;15(4): 559−61.

[14] Black PM, Moriarty T, Alexander E, Stieg P, Woodard EJ, Gleason PL, et al. Development and implementation of intraoperative magnetic resonance imaging and its neurosurgical applications. Neurosurgery 1997;41(4):831−45.

[15] Hadani M, Spiegelman R, Feldman Z, Berkenstadt H, Ram Z. Novel, compact, intraoperative magnetic resonance imaging-guided system for conventional neurosurgical operating rooms. Neurosurgery 2001;48(4):799−809.

[16] Foltynie T, Zrinzo L, Martinez-Torres I, Tripoliti E, Petersen E, Holl E, et al. MRI-guided STN DBS in Parkinson's disease without microelectrode recording: efficacy and safety. J Neurol Neurosurg Psychiatry 2011;82(4):358−63.

[17] Southwell DG, Narvid JA, Martin AJ, Qasim SE, Starr PA, Larson PS. Comparison of deep brain stimulation lead targeting accuracy and procedure duration between 1.5-and 3-tesla interventional magnetic resonance imaging systems: an initial 12-month experience. Stereotact Funct Neurosurg 2016;94(2):102−7.

[18] Chabardes S, Isnard S, Castrioto A, Oddoux M, Fraix V, Carlucci L, et al. Surgical implantation of STN-DBS leads using intraoperative MRI guidance: technique, accuracy, and clinical benefit at 1-year follow-up. Acta Neurochir (Wien) 2015;157(4):729−37.

[19] Starr PA, Markun LC, Larson PS, Volz MM, Martin AJ, Ostrem JL. Interventional MRI−guided deep brain stimulation in pediatric dystonia: first experience with the ClearPoint system. J Neurosurg Pediatr 2014;14(4):400−8.

[20] Chinzei K, Hata N, Jolesz FA, Kikinis R. MR compatible surgical assist robot: system integration and preliminary feasibility study. In: International conference on medical image computing and computer-assisted intervention. Springer, Berlin, Heidelberg; Oct 11, 2000. p. 921−30.

[21] Motkoski JW, Sutherland GR. Why robots entered neurosurgery. Exp Neurosurg Anim Models 2016;85−105.

[22] Golby AJ. Image-guided neurosurgery. Elsevier Science; 2015.

[23] Li G, Su H, Cole GA, Shang W, Harrington K, Camilo A, et al. Robotic system for MRI-guided stereotactic neurosurgery. IEEE Trans Biomed Eng 2015;62(4):1077.

[24] Larson P, Starr PA, Ostrem JL, Galifianakis N, San Luciano Palenzuela M, Martin A. 203 application accuracy of a second generation interventional MRI stereotactic platform: initial experience in 101 DBS electrode implantations. Neurosurgery 2013;60(CN_Suppl. 1):187.

[25] Sidiropoulos C, Rammo R, Merker B, Mahajan A, LeWitt P, Kaminski P, et al. Intraoperative MRI for deep brain stimulation lead placement in Parkinson's disease: 1 year motor and neuropsychological outcomes. J Neurol 2016;263(6):1226−31.

[26] Drane DL, Loring DW, Voets NL, Price M, Ojemann JG, Willie JT, et al. Better object recognition and naming outcome with MRI-guided stereotactic laser amygdalohippocampotomy for temporal lobe epilepsy. Epilepsia 2015;56(1):101−13.

[27] Chittiboina P, Heiss JD, Lonser RR. Accuracy of direct magnetic resonance imaging-guided placement of drug infusion cannulae. J Neurosurg 2015;122(5):1173−9.

[28] Ashkan K, Blomstedt P, Zrinzo L, Tisch S, Yousry T, Limousin-Dowsey P, et al. Variability of the subthalamic nucleus: the case for direct MRI guided targeting. Br J Neurosurg 2007;21(2):197−200.

[29] Patel NK, Plaha P, Gill SS. Magnetic resonance imaging-directed method for functional neurosurgery using implantable guide tubes. Oper Neurosurg 2007;61(Suppl. 5):ONS358−66 p.

[30] Kaouk JH, Goel RK, Haber GP, Crouzet S, Stein RJ. Robotic single-port transumbilical surgery in humans: initial report. BJU Int 2009;103(3): 366−9.

[31] Devito DP, Kaplan L, Dietl R, Pfeiffer M, Horne D, Silberstein B, et al. Clinical acceptance and accuracy assessment of spinal implants guided with SpineAssist surgical robot: retrospective study. Spine 2010;35(24):2109−15.

[32] Antoniou GA, Riga CV, Mayer EK, Cheshire NJ, Bicknell CD. Clinical applications of robotic technology in vascular and endovascular surgery. J Vasc Surg 2011;53(2):493−9.

[33] Masamune K, Kobayashi E, Masutani Y, Suzuki M, Dohi T, Iseki H, et al. Development of an MRI-compatible needle insertion manipulator for stereotactic neurosurgery. J Image Guid Surg 1995;1(4):242−8.

[34] Chinzei K, Kikinis R, Jolesz FA. MR compatibility of mechatronic devices: design criteria. In: International Conference on Medical Image Computing and Computer-Assisted Intervention. Berlin, Heidelberg: Springer; 1999 Sep 19. pp. 1020−30.

[35] Lewin JS, Metzger A, Selman WR. Intraoperative magnetic resonance image guidance in neurosurgery. J Magn Reson Imaging 2000;12(4): 512−24.

[36] Sutherland GR, Maddahi Y, Gan LS, Lama S, Zareinia K. Robotics in the neurosurgical treatment of glioma. Surg Neurol Int 2015;6(Suppl. 1): S1−8.

[37] Sutherland GR, McBeth PB, Louw DF. NeuroArm: an MR compatible robot for microsurgery. International congress series. Elsevier; 2003.

[38] Faria C, Erlhagen W, Rito M, De Momi E, Ferrigno G, Bicho E. Review of robotic technology for stereotactic neurosurgery. IEEE Rev Biomed Eng 2015;8:125−37.

[39] Hawasli AH, Ray WZ, Murphy RK, Dacey Jr RG, Leuthardt EC. Magnetic resonance imaging-guided focused laser interstitial thermal therapy for subinsular metastatic adenocarcinoma: technical case report. Oper Neurosurg 2011;70(Suppl. 2):332−7.

[40] Nycz CJ, Gondokaryono R, Carvalho P, Patel N, Wartenberg M, Pilitsis JG, et al. Mechanical validation of an MRI compatible stereotactic neurosurgery robot in preparation for pre-clinical trials. In: Intelligent Robots and Systems (IROS), 2017 IEEE/RSJ international conference on. IEEE; Sep 24, 2017. p. 1677−84.

[41] Sutherland GR, McBeth PB, Louw DF. NeuroArm: an MR compatible robot for microsurgery. Int Congr Ser 2003;1256:504−8.

[42] Louw DF, Fielding T, McBeth PB, Gregoris D, Newhook P, Sutherland GR. Surgical robotics: a review and neurosurgical prototype development. Neurosurgery 2004;54(3):525−37.

[43] Manjila S, Knudson KE, Johnson Jr C, Sloan AE. Monteris AXiiiS stereotactic miniframe for intracranial biopsy: precision, feasibility, and ease of use. Oper Neurosurg 2015;12(2):119−27.

[44] Mohammadi AM, Hawasli AH, Rodriguez A, Schroeder JL, Laxton AW, Elson P, et al. The role of laser interstitial thermal therapy in enhancing progression-free survival of difficult-to-access high-grade gliomas: a multicenter study. Cancer Med 2014;3(4):971−9.

[45] Comber DB, Pitt EB, Gilbert HB, Powelson MW, Matijevich E, Neimat JS, et al. Optimization of curvilinear needle trajectories for transforamenal hippocampotomy. Oper Neurosurg 2016;13(1):15−22.

[46] Comber DB, Slightam JE, Gervasi VR, Neimat JS, Barth EJ. Design, additive manufacture, and control of a pneumatic MR-compatible needle driver. IEEE Trans Robot 2016;32(1):138−49.

[47] Chinzei K, Miller K, Towards MRI. Towards MRI guided surgical manipulator. Med Sci Monit 2001;7(1):153−63.

[48] Koseki Y, Kikinis R, Jolesz FA, Chinzei K. Precise evaluation of positioning repeatability of MR-compatible manipulator inside MRI. In: International conference on medical image computing and computer-assisted intervention. Springer, Berlin, Heidelberg; 2004. p. 192−9.

[49] Ho M, Kim Y, Cheng SS, Gullapalli R, Desai JP. Design, development, and evaluation of an MRI-guided SMA spring-actuated neurosurgical robot. Int J Robot Res 2015;34(8):1147−63.

[50] Kim Y, Cheng SS, Diakite M, Gullapalli RP, Simard JM, Desai JP. Toward the development of a flexible mesoscale MRI-compatible neurosurgical continuum robot. IEEE Trans Robot 2017;33(6):1386−97.

[51] Cheng SS, Kim Y, Desai JP. New actuation mechanism for actively cooled SMA springs in a neurosurgical robot. IEEE Trans Robot 2017;33: 986−93.

[52] Guo Z, Dong Z, Lee KH, Cheung CL, Fu HC, Ho JD, et al. Compact design of a hydraulic driving robot for intra-operative MRI-guided bilateral stereotactic neurosurgery. IEEE Robot Autom Lett 2018;3(3):2515−22.

[53] Jun C, Lim S, Wolinsky JP, Garzon-Muvdi T, Petrisor D, Cleary K, et al. MR safe robot assisted needle access of the brain: preclinical study. J Med Robot Res 2018;3(01):1850003.

[54] Miyata N, Kobayashi E, Kim D, Masamune K, Sakuma I, Yahagi N, et al. Micro-grasping forceps manipulator for MR-guided neurosurgery. In: International conference on medical image computing and computer-assisted intervention. Springer, Berlin, Heidelberg; Sep 25, 2002. p. 107−13.

[55] Koseki Y, Washio T, Chinzei K, Iseki H. Endoscope manipulator for trans-nasal neurosurgery, optimized for and compatible to vertical field open MRI. In: International conference on medical image computing and computer-assisted intervention. Springer, Berlin, Heidelberg; Sep 25, 2002. p. 114−21.

[56] Raoufi C, Goldenberg AA, Kucharczyk W. Design and control of a novel hydraulically/pneumatically actuated robotic system for MRI-guided neurosurgery. J Biomed Sci Eng 2008;1(01):68.

[57] Hong Z, Yun C, Zhao L, Wang Y. Design and optimization analysis of open-mri compatibile robot for neurosurgery. In: Bioinformatics and biomedical engineering, 2008. ICBBE 2008. The 2nd international conference on 2008 May 16. IEEE. p. 1773−6.

[58] Mattei TA, Rodriguez AH, Sambhara D, Mendel E. Current state-of-the-art and future perspectives of robotic technology in neurosurgery. Neurosurg Rev 2014;37(3):357−66.

[59] Nimsky C, Ganslandt O, Hastreiter P, Fahlbusch R. Intraoperative compensation for brain shift. Surg Neurol 2001;56(6):357−64.

[60] Archip N, Clatz O, Whalen S, Kacher D, Fedorov A, Kot A, et al. Non-rigid alignment of pre-operative MRI, fMRI, and DT-MRI with intraoperative MRI for enhanced visualization and navigation in image-guided neurosurgery. Neuroimage 2007;35(2):609−24.

[61] Škrinjar O, Nabavi A, Duncan J. Model-driven brain shift compensation. Med Image Anal 2002;6(4):361−73.

[62] Hu J, Jin X, Lee JB, Zhang L, Chaudhary V, Guthikonda M, et al. Intraoperative brain shift prediction using a 3D inhomogeneous patient-specific finite element model. J Neurosurg 2007;106(1):164−9.

[63] Tavares WM, Tustumi F, da Costa Leite C, Gamarra LF, Amaro Jr E, et al. An image correction protocol to reduce distortion for 3-T stereotactic MRI. Neurosurgery 2013;74(1):121−7.

[64] Baldwin LN, Wachowicz K, Thomas SD, Rivest R, Fallone BG. Characterization, prediction, and correction of geometric distortion in MR images. Med Phys 2007;34(2):388−99.

[65] Mallozzi R. Geometric distortion in MRI. The Phantom Laboratory, Inc.; 2015.

[66] Walker A, Liney G, Metcalfe P, Holloway L. MRI distortion: considerations for MRI based radiotherapy treatment planning. Australas Phys Eng Sci Med 2014;37(1):103−13.

[67] Murgasova M, Estrin GL, Rutherford M, Rueckert D, Hajnal J. Distortion correction in fetal EPI using non-rigid registration with Laplacian constraint. In: Biomedical Imaging (ISBI), 2016 IEEE 13th international symposium on 2016 Apr 13. IEEE. p. 1372−5.

[68] Kwok KW, Chow GC, Chau TC, Chen Y, Zhang SH, Luk W, et al. FPGA-based acceleration of MRI registration: an enabling technique for improving MRI-guided cardiac therapy. J Cardiovasc Magn Reson 2014;16(1):W11.

[69] Kwok KW, Chen Y, Chau TC, Luk W, Nilsson KR, Schmidt EJ, et al. MRI-based visual and haptic catheter feedback: simulating a novel system's contribution to efficient and safe MRI-guided cardiac electrophysiology procedures. J Cardiovasc Magn Reson 2014;16(1):O50.

[70] Gu X, Pan H, Liang Y, Castillo R, Yang D, Choi D, et al. Implementation and evaluation of various demons deformable image registration algorithms on a GPU. Phys Med Biol 2009;55(1):207.

[71] Bhushan C, Haldar JP, Choi S, Joshi AA, Shattuck DW, Leahy RM. Co-registration and distortion correction of diffusion and anatomical images based on inverse contrast normalization. Neuroimage 2015;115:269−80.

[72] Moche M, Trampel R, Kahn T, Busse H. Navigation concepts for MR image-guided interventions. J Magn Reson Imaging 2008;27(2):276−91.

34. Stereotactic NeuroSurgery

[73] Chavhan GB, Babyn PS, Thomas B, Shroff MM, Haacke EM. Principles, techniques, and applications of T2*-based MR imaging and its special applications. Radiographics 2009;29(5):1433−49.

[74] Elayaperumal S, Plata JC, Holbrook AB, Park YL, Pauly KB, Daniel BL, et al. Autonomous real-time interventional scan plane control with a 3-D shape-sensing needle. IEEE Trans Med Imaging 2014;33(11):2128−39.

[75] Strother SC, Anderson JR, Xu XL, Liow JS, Bonar DC, Rottenberg DA. Quantitative comparisons of image registration techniques based on high-resolution MRI of the brain. J Comput Assist Tomogr 1994;18(6):954−62.

[76] Wang D, Strugnell W, Cowin G, Doddrell DM, Slaughter R. Geometric distortion in clinical MRI systems: Part I: Evaluation using a 3D phantom. Magn Reson Imaging 2004;22(9):1211−21.

[77] Dumoulin C, Souza S, Darrow R. Real-time position monitoring of invasive devices using magnetic resonance. Magn Reson Med 1993;29(3): 411−15.

[78] Werner R, Krueger S, Winkel A, Albrecht C, Schaeffter T, Heller M, et al. MR-guided breast biopsy using an active marker: a phantom study. J Magn Reson Imaging 2006;24(1):235−41.

[79] Zimmermann H, Müller S, Gutmann B, Bardenheuer H, Melzer A, Umathum R, et al. Targeted-HASTE imaging with automated device tracking for MR-guided needle interventions in closed-bore MR systems. Magn Reson Med 2006;56(3):481−8.

[80] Coutts GA, Gilderdale DJ, Chui M, Kasuboski L, Desouza NM. Integrated and interactive position tracking and imaging of interventional tools and internal devices using small fiducial receiver coils. Magn Reson Med 1998;40(6):908−13.

[81] Konings MK, Bartels LW, Smits HF, Bakker CJ. Heating around intravascular guidewires by resonating RF waves. J Magn Reson Imaging 2000;12(1):79−85.

[82] Rube MA, Holbrook AB, Cox BF, Houston JG, Melzer A. Wireless MR tracking of interventional devices using phase-field dithering and projection reconstruction. Magn Reson Imaging 2014;32(6):693−701.

[83] Wang W, Dumoulin CL, Viswanathan AN, Tse ZT, Mehrtash A, Loew W, et al. Real-time active MR-tracking of metallic stylets in MR-guided radiation therapy. Magn Reson Med 2015;73(5):1803−11.

[84] Richardson RM, Kells AP, Martin AJ, Larson PS, Starr PA, Piferi PG, et al. Novel platform for MRI-guided convection-enhanced delivery of therapeutics: preclinical validation in nonhuman primate brain. Stereotact Funct Neurosurg 2011;89(3):141−51.

[85] Truwit C, Martin AJ, Hall WA. MRI guidance of minimally invasive cranial applications. Interventional magnetic resonance imaging. Springer; 2011. p. 97−112.

[86] Weiss S, Kuehne T, Brinkert F, Krombach G, Katoh M, Schaeffter T, et al. In vivo safe catheter visualization and slice tracking using an optically detunable resonant marker. Magn Reson Med 2004;52(4):860−8.

[87] Krieger A, Song SE, Cho NB, Iordachita II, Guion P, Fichtinger G, et al. Development and evaluation of an actuated MRI-compatible robotic system for MRI-guided prostate intervention. IEEE/ASME Trans Mechatron 2013;18(1):273−84.

[88] El Bannan K, Chronik BA, Salisbury SP. Development of an MRI-compatible, compact, rotary-linear piezoworm actuator. J Med Device 2015;9(1):014501.

[89] Wang Y, Cole GA, Su H, Pilitsis JG, Fischer GS. MRI compatibility evaluation of a piezoelectric actuator system for a neural interventional robot. In: Engineering in Medicine and Biology Society, 2009. EMBC 2009. Annual international conference of the IEEE. IEEE; Sep 3, 2009. p. 6072−5.

[90] Su H, Cardona DC, Shang W, Camilo A, Cole GA, Rucker DC, et al. A MRI-guided concentric tube continuum robot with piezoelectric actuation: a feasibility study. In: Robotics and Automation (ICRA), 2012 IEEE international conference on 2012 May 14. IEEE. p. 1939−45.

[91] Stoianovici D, Patriciu A, Petrisor D, Mazilu D, Kavoussi L. A new type of motor: pneumatic step motor. IEEE/ASME Trans Mechatron 2007;12(1):98−106.

[92] Sajima H, Kamiuchi H, Kuwana K, Dohi T, Masamune K. MR-safe pneumatic rotation stepping actuator. J Robot Mechatron 2012;24(5): 820−7.

[93] Chen Y, Mershon CD, Tse ZT. A 10-mm MR-conditional unidirectional pneumatic stepper motor. IEEE/ASME Trans Mechatron 2015;20(2): 782−8.

[94] Chen Y, Kwok KW, Tse ZTH. An MR-conditional high-torque pneumatic stepper motor for MRI-guided and robot-assisted intervention. Ann Biomed Eng 2014;42:1823−33.

[95] Su H, Cole GA, Fischer GS. High-field MRI-compatible needle placement robots for prostate interventions: pneumatic and piezoelectric approaches. Adv Robot Virtual Real 2012;3−32.

[96] Sutherland GR, Latour I, Greer AD, Fielding T, Feil G, Newhook P. An image-guided magnetic resonance-compatible surgical robot. Neurosurgery 2008;62(2):286−93.

[97] Sutherland GR, Latour I, Greer AD. Integrating an image-guided robot with intraoperative MRI. IEEE Eng Med Biol Mag 2008;27(3):59−65.

[98] Stoianovici D, Kim C, Petrisor D, Jun C, Lim S, Ball MW, et al. MR safe robot, FDA clearance, safety and feasibility of prostate biopsy clinical trial. IEEE/ASME Trans Mechatron 2017;22(1):115−26.